Fluctuations in Jupiter's Equatorial Stratospheric Oscillation

Arrate Antuñano[a,*], Richard G. Cosentino[b,c], Leigh N. Fletcher[a], Amy Simon[c], Thomas Greathouse[d], Glenn Orton[e]

[a] *School of Physics and Astronomy, University of Leicester, Leicester, LE1 7RH (U.K.)*
[b] *Department of Astronomy, University of Maryland, College Park, MD 20742 (U.S.A.)*
[c] *NASA Goddard Space Flight Center, Solar System Exploration Div., NASA/GSFC, Greenbelt, MD 20771 (U.S.A.)*
[d] *Southwest Research Institute, San Antonio, TX 78238 (U.S.A.)*
[e] *Jet Propulsion Laboratory, Pasadena, CA 91109 (U.S.A.)*

The equatorial stratospheres of the Earth, Jupiter, and Saturn all exhibit a remarkable periodic oscillation of their temperatures and winds with height. Earth's Quasi-Biennial Oscillation (QBO) and Saturn's Quasi-Periodic Equatorial Oscillation (QPO) have recently been observed to experience disruptions in their vertical structure as a consequence of atmospheric events occurring far from the equator. Here we reveal that Jupiter's Quasi-Quadrennial Oscillation (QQO) can also be perturbed by strong tropospheric activity at the equatorial and off-equatorial latitudes. Observations of Jupiter's stratospheric temperatures between 1980 and 2011 show two significantly different periods for the QQO, with a 5.7-year period between 1980 and 1990 and a 3.9-year period between 1996 and 2006. Major disruptions to the predicted QQO pattern in 1992 and 2007 coincided with dramatic planetary-scale disturbances in the equatorial and low-latitude troposphere, suggesting that they are connected to vertically propagating waves generated by meteorological sources in the deeper troposphere (i.e. 500-4000 mbar pressures). Disruptions in Jupiter's periodic oscillations are thus inherently different than those at Saturn or the Earth. This interconnectivity between the troposphere and stratosphere that is likely common to all planetary atmospheres shows that seemingly regular cycles of variability can switch between different modes when subjected to extreme meteorological events.

The observed equatorial stratospheric oscillations on Earth, Jupiter, and Saturn, are thought to be linked to waves propagating upwards from the deeper atmosphere. Tropospheric convection produces a spectrum of waves that propagate into the stratosphere, where they can interact with the background winds and potentially break, depositing angular momentum into the zonal jets (1; 2; 3). Once thought to be regular and stable, recent observations have shown that such oscillations are dis-

*Corresponding author
Email address: aam58@leicester.ac.uk (Arrate Antuñano)

rupted by horizontally propagating stratospheric waves on both Earth and Saturn. Earth's QBO (4) recently experienced an anomalous, very short reversal period of only nine months, as compared to the mean of 28 months observed over the last 40 years of observations (5; 6). This odd behaviour of the QBO was attributed to large amounts of wave activity originating from higher latitudes, moving horizontally equatorwards and penetrating farther south than normal. This disruption of Earth's QBO may be partially related to the weakening of meridional temperature gradients attributed to climate change (6; 5) or to extreme El Niño events (7). After this disruption the QBO re-established into its nominal 28-month mean period (6). Saturn's QPO (8; 3), observed with a $\sim$ 15-year periodicity, was disrupted between 2011-2014 (9). An energetic convective storm erupted in 2010 at northern mid-latitudes (10; 11; 12), spawning a large, hot stratospheric vortex that persisted for 3 years near $\sim 40°$ N (all latitudes in this paper are planetocentric) (13). Waves emanating from this source traveled over 30,000 km to the equator, perturbing the QPO (9).

Yearly infrared observations of Jupiter's QQO (1; 14) in the 1980s and 1990s estimated that the equatorial stratospheric temperatures oscillate with a 4-5-year periodicity (15; 16). This was confirmed by a later study (17) that reported a 4.5-year periodicity of the QQO between 1980 and 2000. The increase of the data points in the temporal sampling and the addition of a subsequent decade of observations enables a more careful assessment of the supposed regularity of Jupiter's QQO. At higher pressures in the troposphere, several types of large-scale semi-regular events (plume outbreaks; fades, revivals and expansions of belts, and other disturbances) can alter the banded morphology of clouds in Jupiter's weather layer (18).

Here we characterized the long-term behavior of the QQO using ground-based infrared images acquired over almost three Jovian years (1980-2011) at the Infrared Telescope Facility (IRTF) on Maunakea, Hawai'i, at 7.6-7.9 μm sensing the 10-20 mbar pressure level (where the stratospheric temperature oscillations are observed). We employed a wavelet transform analysis and a non-linear least-squares curve-fitting analysis to characterize the long-term periodicity of the stratospheric brightness temperature oscillations, and determine whether, like the Earths QBO or Saturns QPO, the QQO can be disrupted by tropospheric convective events and/or stratospheric perturbations (see Methods). An analysis of previously reported tropospheric meteorological activity, and of the longitudinal variance of the stratospheric brightness temperatures at the equatorial and off-equatorial latitudes were also carried out to investigate the origin of the QQO disruptions.

Long-term QQO Periodicity Analysis

Figure 1e and Figure 1f show the $\sim$ 7.9-μm brightness temperature and its temporal variance between $\pm 30°$ latitude for the 31 years analyzed in this study, showing the dynamic nature of Jupiter's stratospheric temperatures. The QQO signal is clearly observed with temperatures at the equator oscillating in time between relatively lower and higher values, anti-correlated with those at approximately $\pm 12°$ latitude, as suggested by (1; 14). The variance of the temperatures for the entire observational data set shows that the QQO signal is most prominent between $\pm 4°$ of the equator and at 12-14° north and south latitudes, in agreement with (19). The significant temporal variance found at 26° N is not part of the QQO and represents the large stratospheric variability of the North Temperate Belt (NTB) due to the presence of stratospheric wave activity (14; 20). Figure 1 provides our first hint that Jupiter's temperature oscillations have been disrupted at certain times, having a longer period between 1980 and 1990 and a shorter period between 1996 and 2006. This change in the QQO periodicity is better seen in Figure 1g, where the brightness temperature of the equatorial latitudes between $\pm 1°$ is shown. Thus, just like the QBO on Earth and the QPO on Saturn, the QQO on Jupiter could have also been modified by strong meteorological activity. However, unlike Earth, Jupiter's QQO appears to have been locked into a different period between 1996 and 2006, compared to 1980-1990. This change in the period has never been observed for Earth's QBO, which returned to the usual 28-month mean period after the 2016 disruption (6). Observations of Saturn over more than a decade would be needed to know whether the 2011-13 disruption of the QPO (9) had the same effect. However, a preliminary assessment by (21) suggest that the QPO returned to the same 15-year phase after the disturbance.

To understand how the periodicity observed in Figure 1 changes, we employed both a wavelet-transform analysis and a non-linear least-squares curve-fitting analysis. Detailed information of these techniques are described in Methods. In Figure 2 the power spectrum of the stratospheric temperature variability over time for the equatorial latitudes between $\pm 1°$ and 11-13°, north and south, are shown. The QQO is clearly observed, particularly during 1980-1988 and 1996-2006, with significantly different periods, both at the equatorial and off-equatorial latitudes. At the equator, the wavelet-transform analysis shows predominant periods of $5.0^{+1.8}_{-1.0}$ years between 1980 and 1988 and 3.9 ± 0.7 years between 1995 and 2006 (see Figure 2d). Between 1989-1994 and 2007-2011, when the QQO signal becomes irregular and disorganised, no significant periodicity is observed. In short, Jupiter's equatorial oscillation should not be described as "quadrennial" at all as we do not know what the nominal period is. (1; 14; 19) reported a potential anticorrelation of the stratospheric temperatures between the equatorial and off-equatorial latitudes, which is confirmed in Figure 1. However, at 12° N and 12° S the period seems to vary between $\sim 7-7.5$ years and $3-4$ years, maybe due to weaker meridional temperature gradients making the off-equatorial latitudes susceptible to localized convective weather events. The variability of the period of the off-equatorial latitudes is most prominent in the northern hemisphere, where the wavelet-transform analysis shows a dominant 7-8-year periodicity between 1986 and 2000, compared to the $\sim$ 3-year periodicity found in 1980-1986 and 2000-2006. The observed larger periodicity at the off-latitudes might not be associated with the QQO and could be part of a completely different phenomena, like the Earth's Semi-Annual Oscillations (SAO) (22) observed at the equatorial and tropical upper stratosphere. However, further observations will be needed to understand the nature of these larger periodicities and their relation to the QQO. All the results from the wavelet-transform analysis are shown in Table 1.

To add more confidence to the two discrete periods at the equatorial latitudes, Figure 3 showcases the non-linear Levenberg-Marquardt method to derive the best sinusoidal modeled amplitude, period, phase, and offset constant to represent the time series. This confirms the wavelet analysis in the previous figure, and shows how well the newly-proposed periods fit the data (see Extended Data Figure 1) for the fits at the off-equatorial latitudes). Model 1 attempts to reproduce the initial QQO discovery by fitting only the data between 1980 and 1990, where previous studies estimated the QQO period to be ∼4-5 years (1; 14). However, additional observations added to our study reveal an equatorial QQO period of $5.7^{+1.1}_{-0.8}$ years for this time interval. Model 4 was developed to fit only the data between 1996 and 2006, revealing a 3.9 ± 0.2-year period, a statistically different period to that found in Model 1 for 1980-1990. This change in the QQO period between 1980-1990 and 1996-2006 is larger than the 20% variability usually observed at the Earth's QBO (2). Model 2 attempts to fit data that span from 1980 to late 2000 (23), and reproduces an approximate 4.5-year QQO period consistent with analysis done by (17). However, this model does not adequately fit the observations mainly before 1992 where the model phase departs from the data by almost 180°. Model 3 fits the observations between 1990 and late 2011, finding a 4.2-year period. However, this latter model does not adequately reproduce the 2007-2008 data, with the 2008 observations departing by 180° from the model phase. If Jupiter's QQO had precisely followed the periodicities derived by our model, then local temperature minima were expected to be observed in 1991-1992 and late 2007-2008. However, the observations from these epochs show the complete opposite, with a stratosphere ~ 3 K warmer than expected, displaying instead early temperature maxima. Our observations also show that the QQO signal is not just delayed during these two epochs (for example, slowing down the descending pattern of temperature anomalies for a short time), but instead it becomes irregular and disorganised over a longer time span. Understanding how Jovian tropospheric and stratospheric activity could have disturbed the QQO during these two epochs is essential to further our knowledge in the vertical coupling of the gas giant atmosphere.

Disruption Origins

The abrupt change observed in Earth's QBO has been partially attributed to weaker temperature gradients from a changing climate and to an extreme El Niño event, where stratospheric waves from higher latitudes could propagate further towards the equator and affect the regular descent of the jets (6; 5; 7). Jupiter's climate, however, is unlikely to be changing, and given its low obliquity there are few similarities between the abrupt change in Earth's QBO and the QQO disruptions discovered here. Jupiter does, however, exhibit a plethora of energetic and convective events at multiple latitudes, and if these events serve to weaken latitudinal temperature contrasts, then they might alter the transmissivity of the atmosphere to wave propagation, allowing waves from higher latitudes to reach, and possibly alter, the QQO region. Pursuing this hypothesis, we investigated the temperature gradients in Figure 1, focusing on higher latitudes away from the off-equatorial jets, postulating that energetic events associated with the 21° N jet (24; 25) might produce significant waves that could alter the QQO. However, the meridional temperature gradient with respect to latitude (shown in Extended Data Figure 2) indicates no clear behavioral changes near to the disruptive events of 1992 and 2007, either before or after.

Saturn's QPO was disrupted by strong convective activity at northern mid-latitudes that produced a large, hot stratospheric anticyclone (9). Waves emitted by this unusual phenomenon are thought to have propagated horizontally through the stratosphere to modify the equatorial oscillation (9). Similarly, (26) reported that Earth's QBO disruption was associated with record stratospheric tropical wave activity. We therefore searched for similar hot stratospheric vortices and strong stratospheric wave activity that could have disrupted Jupiter's QQO, by analysing the longitudinal variance of the 7.9-μm brightness temperature at the equatorial and tropical latitudes between 1980 and 2011 (see Methods for a detailed description). The variance as a function of latitude and date is shown in Figure 4. High variance would indicate the presence of either stratospheric vortices or wave-patterns that could potentially alter the QQO, while low variance would be indicative of either a quiescent state of the stratosphere or a homogeneously-warm latitudinal band. Figure 4 shows that during the dates preceding the 2007 QQO disruption, the variance at tropical and equatorial latitudes was very low with no signs of stratospheric vortices or other significant perturbations. This reveals that the physical phenomena perturbing the QQO are completely different from that observed on Earth and Saturn. Unfortunately, the limited observations in 1991 and 1992 do not enable us to confidently compute the longitudinal variance during that disruption event. This study also shows that the largest longitudinal variability at the tropical latitudes is unexpectedly found at the times when the QQO was most prominent (i.e. 1980-1990 and 1996-2005). These large variabilities correspond to the presence of (i) tropospheric wave activity usually observed at the northern boundary of the North Equatorial Belt at 16-18° N (27), and (ii) stratospheric wave activity over the North Temperate Belt at 21-27° N (14). Unlike the energetic stratospheric activity that disrupted the QBO on Earth and the QPO on Saturn, these are not one-off events and are commonly observed on Jupiter. Given that the equatorial stratospheric temperature oscillations are thought to be driven by vertically-propagating waves, rather than by waves propagating horizontally (i.e., meridionally), it is hard to determine whether this correlation between a prominent QQO and the presence of strong extra-tropical stratospheric variability is a mere coincidence, or is revealing something about the dynamical processes sustaining the regular oscillations. Future numerical modelling work, and extension of the observational time series, are highly desirable to address this question.

The anomalous QQO period changes observed in 1992 and 2007 coincided with dramatic planetary scale disturbances observed much deeper in Jupiter's troposphere (500-4000 mbar compared to 10-20 mbar) at equatorial and tropical latitudes during 1990-1992 and 2006-2007. During these two epochs, nearly-contemporaneous disturbances occurred at equatorial and tropical latitudes completely altering Jupiter's banded cloud morphology. These were part of rare events known as 'Global Upheavals' (28; 29) that usually involve multiple energetic convective events in the cloud decks. Between 1990-1992 and 2006-2007, these Global Upheavals involved three different types of tropospheric activity:

1. Convective outbreaks at the zonal jet at 21° N in early 1990 and 2007 (25; 30; 31; 32). Observations of these vigorous outbreaks showed that they completely altered the coloration of the North Temperate Belt (i.e. 21° - 28° N) at visible wavelengths, sensing the $\sim$700 mbar pressure level, while no changes were observed in the stratosphere (32) or deeper in the troposphere (33).
2. Equatorial Zone (EZ) disturbances at $\pm 7°$ between January and April 1992 and April 2006 and September 2007 (34; 33). These were part of a quasi-periodic pattern of cloud-clearing events that completely altered the appearance at the EZ at the $\sim$700 mbar pressure level (visible wavelengths) and at the 1-4 bar level (5 μm wavelength). During these events the usually visibly-white and 5-μm dark Equatorial Zone appeared visibly-dark and 5-μm bright. Observations at 2.12 μm, sensing stratospheric hazes, of the same epochs showed a complex temporal variability not related to the EZ disturbances, suggesting that the EZ disturbances were confined to the cloud deck.
3. South Equatorial Belt fading and revival cycles at $7 - 17°$ S in 1989-1990, 1992-1993 and 2007 (35; 36; 37; 38; 39; 29; 40; 41). These events were observed to dramatically alter the troposphere at 500 mbar - 4 bar pressure levels without altering the stratosphere (12).

The contemporaneity of the disruptions of the stratospheric QQO and the anomalies observed at tropospheric levels suggest that, unlike on Earth and Saturn, disruptions of Jupiter's stratospheric temperature oscillations are not limited to horizontally propagating waves from large stratospheric perturbations at higher latitudes. Instead, the QQO period is highly sensitive to tropospheric meteorology, indicative of strong coupling between the troposphere and stratosphere. However, previous studies of the NTB outbreaks and the EZ disturbances reported these events to occur quasi-periodically with a 5-year (28) and 7-year (34; 33) intervals, something not observed in the QQO disruptions. We therefore suggest that vertically propagating waves from a chain of these disturbances in the weather layer (i.e., the 'global upheaval', rather than an individual tropospheric event) could be responsible for the disruptions of the QQO and the change in its periodicity.

Discussion

The distinction between the disruption mechanisms for the Earth's and Saturn's oscillations (horizontally propagating waves from strong stratospheric wave activity) and the Jovian one (vertically propagating waves from energetic tropospheric activity) provides a new constraint on numerical atmospheric simulations of disturbed equatorial oscillations in planetary atmospheres, as tropospheric wave creation mechanisms can easily be reproduced while Saturn's hot stratospheric vortex remains nearly impossible to model. The lock of Jupiter's equatorial stratospheric temperature oscillation into different phases and periods that differ by more than 20% (a phenomenon not witnessed on Earth or Saturn) means that it cannot be accurately described as quadrennial. Indeed, we propose that these phenomena should be more generically referred to as the JESO and SESO (Jupiter Equatorial Stratospheric Oscillation and Saturn Equatorial Stratospheric Oscillation), so as not to directly imply their periods. We hope that future observations might be able to determine whether or not a UESO (Uranus) or a NESO (Neptune) also exist. We predict that future global-scale upheavals will similarly perturb Jupiter's QQO into a new phase and period, and will seek to test this hypothesis via continued monitoring of variable phenomena in the Jovian atmosphere.

References

[1] Leovy, C. B., Friedson, A. J. & Orton, G. S. The quasiquadrennial oscillation of Jupiter's equatorial stratosphere. *Nature* **354**, 380–382 (1991).

[2] Baldwin, M. P. *et al.* The quasi-biennial oscillation. *Rev. Geophys.* **39**, 179–230 (2001).

[3] Fouchet, T. *et al.* An equatorial oscillation in Saturn's middle atmosphere. *Nature* **453**, 200–202 (2008).

[4] Lindzen, R. S. & Holton, J. R. A Theory of the Quasi-Biennial Oscillation. *J. Atmos. Sci.* **25**, 1095–1107 (1968).

[5] Newman, P. A., Coy, L., Pawson, S. & Lait, L. R. The anomalous change in the qbo in 20152016. *Geophys. Res. Lett.* **43**, 8791–8797 (2016). URL `http://dx.doi.org/10.1002/2016GL070373`. 2016GL070373.

[6] Osprey, S. M. *et al.* An unexpected disruption of the atmospheric quasi-biennial oscillation. *Science* **353**, 1424–1427 (2017). URL `http://science.sciencemag.org/content/353/6306/1424`. `http://science.sciencemag.org/content/353/6306/1424.full.pdf`.

[7] Barton, C. & McCormack, J. Origin of the 2016 qbo disruption and its relationship to extreme el niño events. *Geophys. Res. Lett.* **44**, 11–150 (2017).

[8] Orton, G. S. *et al.* Semi-annual oscillations in Saturn's low-latitude stratospheric temperatures. *Nature* **453**, 196–199 (2008).

[9] Fletcher, L. N. *et al.* Disruption of Saturn's quasi-periodic equatorial oscillation by the great northern storm. *Nature Astronomy* **1**, 765–770 (2017).

[10] Sánchez-Lavega, A. *et al.* Deep winds beneath saturns upper clouds from a seasonal long-lived planetary-scale storm. *Nature* **475**, 71 (2011).

[11] Fischer, G. *et al.* A giant thunderstorm on saturn. *Nature* **475**, 75 (2011).

[12] Fletcher, L. N. *et al.* Thermal structure and dynamics of saturns northern springtime disturbance. *Science* **332**, 1413–1417 (2011).

[13] Fletcher, L. N. *et al.* The origin and evolution of saturn's 2011–2012 stratospheric vortex. *Icarus* **221**, 560–586 (2012).

[14] Orton, G. S. *et al.* Thermal maps of Jupiter - Spatial organization and time dependence of stratospheric temperatures, 1980 to 1990. *Science* **252**, 537–542 (1991).

[15] Orton, G. S. *et al.* Spatial Organization and Time Dependence of Jupiter's Tropospheric Temperatures, 1980-1993. *Science* **265**, 625–631 (1994).

[16] Friedson, A. J. New Observations and Modelling of a QBO-Like Oscillation in Jupiter's Stratosphere. *Icarus* **137**, 34–55 (1999).

[17] Simon-Miller, A. A. *et al.* Jupiter's atmospheric temperatures: From Voyager IRIS to Cassini CIRS. *Icarus* **180**, 98–112 (2006).

[18] Fletcher, L. N. *et al.* Moist Convection and the 2010-2011 Revival of Jupiter's South Equatorial Belt. *ArXiv e-prints* (2017). `1701.00965`.

[19] Cosentino, R. G. *et al.* New observations and modeling of jupiter's quasi-quadrennial oscillation. *J. Geophys. Res.* n/a–n/a (2017). URL `http://dx.doi.org/10.1002/2017JE005342`. 2017JE005342.

[20] Fletcher, L. N. *et al.* Mid-infrared mapping of Jupiter's temperatures, aerosol opacity and chemical distributions with IRTF/TEXES. *Icarus* **278**, 128–161 (2016). `1606.05498`.

[21] Guerlet, S. *et al.* Equatorial oscillation and planetary wave activity in saturn's stratosphere through the cassini epoch. *J. Geophys. Res.* **123**, 246–261 (2018).

[22] Garcia, R. R., Dunkerton, T. J., Lieberman, R. S. & Vincent, R. A. Climatology of the semiannual oscillation of the tropical middle atmosphere. *J. Geophys. Res.* **102**, 26019–26032 (1997).

[23] Flasar, F. M. *et al.* An intense stratospheric jet on Jupiter. *Nature* **427**, 132–135 (2004).

[24] Peek, B. M. *The Planet Jupiter* (Faber and Faber, London, 1958).

[25] Sanchez-Lavega, A., Miyazaki, I., Parker, D., Laques, P. & Lecacheux, J. A disturbance in jupiter's high-speed north temperate jet during 1990. *Icarus* **94**, 92–97 (1991).

[26] Coy, L., Newman, P. A., Pawson, S. & Lait, L. R. Dynamics of the disrupted 2015/16 quasi-biennial oscillation. *J. Clim* **30**, 5661–5674 (2017).

[27] Fletcher, L. *et al.* Jupiter's north equatorial belt expansion and thermal wave activity ahead of juno's arrival. *Geophys. Res. Lett.* **44**, 7140–7148 (2017).

[28] Rogers, J. H. *The giant planet Jupiter*, vol. 6 (Cambridge University Press, 1995).

[29] Rogers, J. H. The climax of jupiter's global upheaval. *BAA* **117**, 226–230 (2007).

[30] Rogers, J. Jupiter in 1989-90. *BAA* **102**, 135–150 (1992).

[31] García-Melendo, E., Sánchez-Lavega, A. & Dowling, T. E. Jupiter's 24° n highest speed jet: Vertical structure deduced from nonlinear simulations of a large-amplitude natural disturbance. *Icarus* **176**, 272–282 (2005).

[32] Sánchez-Lavega, A. *et al.* Depth of a strong jovian jet from a planetary-scale disturbance driven by storms. *Nature* **451**, 437 (2008).

[33] Antuñano, A. *et al.* Jupiter's atmospheric variability from long-term ground-based observations at 5 μm. *Astron. J.* **158**, 130 (2019). URL `https://doi.org/10.3847%2F1538-3881%2Fab2cd6`.

[34] Antuñano, A. *et al.* Infrared characterization of jupiter's equatorial disturbance cycle. *Geophys. Res. Lett.* **45**, 10–987 (2018).

[35] Yanamandra-Fisher, P., Orton, G. & Friedson, J. Time dependence of jupiter's tropospheric temperatures and cloud properties: The 1989 seb disturbance. In *Bull. Amer. Astron. Soc.*, vol. 24, 1039 (1992).

[36] Kuehn, D. & Beebe, R. A study of the time variability of jupiter's atmospheric structure. *Icarus* **101**, 282–292 (1993).

[37] Satoh, T. & Kawabata, K. A change of upper cloud structure in jupiter's south equatorial belt during the 1989–1990 event. *J. Geophys. Res.* **99**, 8425–8440 (1994).

[38] Sánchez-Lavega, A. & Gomez, J. The south equatorial belt of jupiter, i: Its life cycle. *Icarus* **121**, 1–17 (1996).

[39] Moreno, F., Molina, A. & Ortiz, J. The 1993 south equatorial belt revival and other features in the jovian atmosphere: an observational perspective. *Astron. Astrophys* **327**, 1253–1261 (1997).

[40] Rogers, J. H. Jupiter embarks on a'global upheaval'. *BAA* **117**, 113–115 (2007).

[41] Reuter, D. C. *et al.* Jupiter Cloud Composition, Stratification, Convection, and Wave Motion: A View from New Horizons. *Science* **318**, 223 (2007).

[42] Fletcher, L. *et al.* Retrievals of atmospheric variables on the gas giants from ground-based mid-infrared imaging. *Icarus* **200**, 154–175 (2009).

[43] Torrence, C. & Compo, G. P. A practical guide to wavelet analysis. *Bull. Amer. Astron. Soc.* **79**, 61–78 (1998).

[44] Scargle, J. D. Studies in astronomical time series analysis. ii-statistical aspects of spectral analysis of unevenly spaced data. *Astron. J.* **263**, 835–853 (1982).

[45] Chapa, S. R., Rao, V. B. & Prasad, G. S. S. D. Application of wavelet transform to meteosat-derived cold cloud index data over south america. *Mon Weather Rev* **126**, 2466–2481 (1998).

[46] Huang, N. E. *et al.* The empirical mode decomposition and the hilbert spectrum for nonlinear and non-stationary time series analysis. *P Roy Soc A-Math Phy* **454**, 903–995 (1998).

Acknowledgement

AA and LNF are supported by a European Research Council Consolidator Grant under the European Union's Horizon 2020 research and innovation program, grant agreement number 723890, at the University of Leicester. LNF is also supported by a Royal Society Research Fellowship. RGC research was supported by an appointment to the NASA Postdoctoral Program at the NASA Goddard Space Flight Center, administered by Universities Space Research Association under contract with NASA. GSO was supported by grants from the National Aeronautics and Space Administration to the Jet Propulsion Laboratory, California Institute of Technology. AAS was supported by grants from the Space Telescope Science Institute, which is operated by the Association of Universities for

Research in Astronomy, Inc., under NASA contract NAS 5-26555. TG was funded in part by a NASA SSO sub-grant through JPL as well as by NASA PAST grant NNX14AG34G.

Author Contributions

AA was responsible for reducing and calibrating all the data, performing the wavelet-transform analysis and writing the article. RGC performed the non-linear Levenberg-Marquardt, analyzed the temperature gradients and helped writing the article. GSO, AAS, TG and LNF were responsible for or assisted with the ground-based observations and helped with the discussion. All authors read and commented on the manuscript.

Competing Financial Interests

The authors declare no competing financial interests.

Data Availability

This work relies on ground-based data acquired at the Infrared Telescope Facility (IRTF) on Maunakea, Hawai'i. Jupiter images at 7.6-7.9 μm are available from the primary author A Antuñano and from L N Fletcher, and are in the process of being archived with NASA's Planetary Data System. The cylindrical maps and the emission angle files used in this study to compute the zonal-mean brightness temperatures can be found in `https://doi.org/10.5281/zenodo.3764712`.

341 **Figures and Tables:**

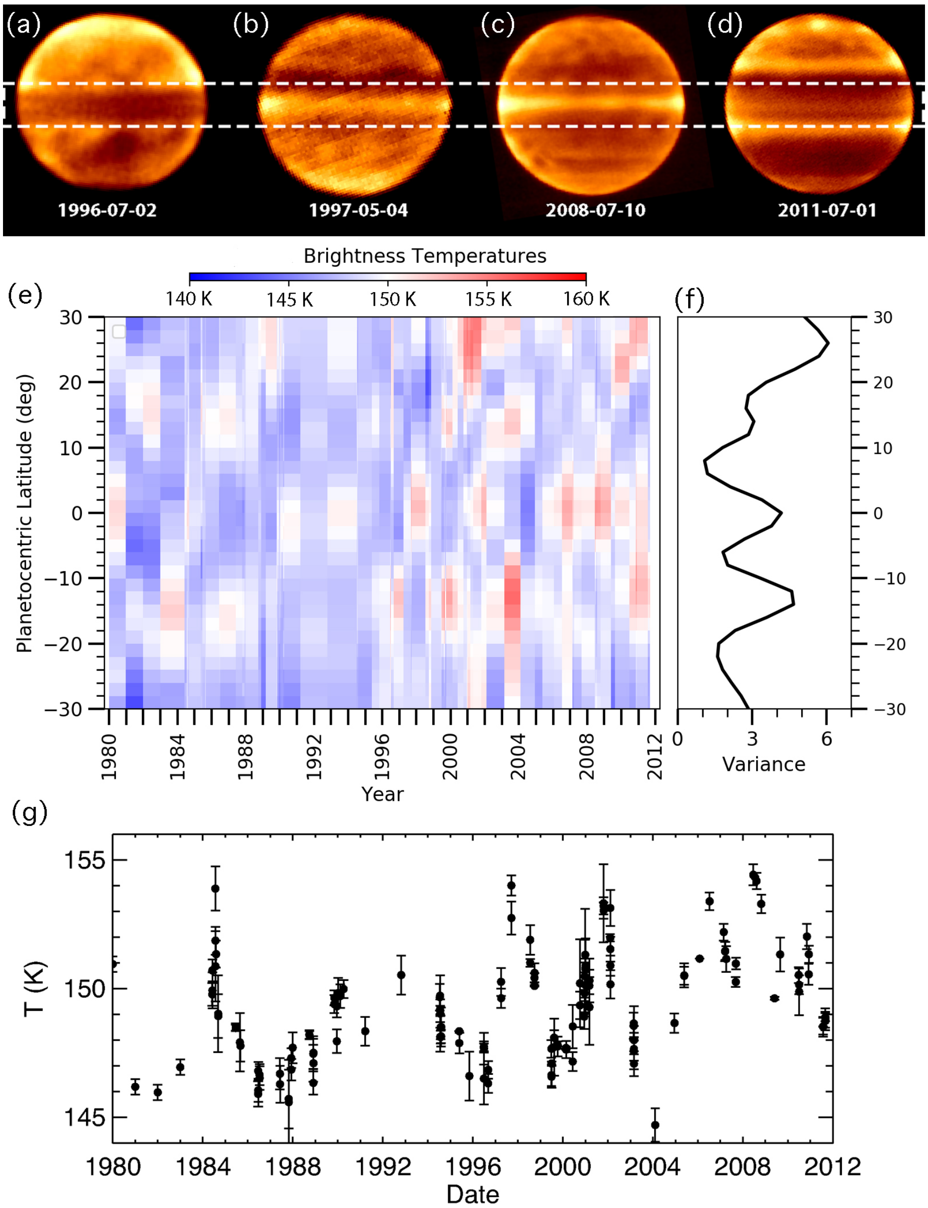

Figure 1: Four examples of Jupiter observations at ~ 7.9 μm captured by the MIRLIN instrument on NASA's Infrared Telescope Facility (IRTF) on 2 July 1996 (a) and 4 May 1997 (b) and by IRTF/MIRSI on 10 July 2008 (c) and 1 July 2011 (d), showing the variation in the stratospheric temperatures at the equator and tropics. Radiances in (a-d) are converted to brightness temperatures in (e), showing equatorial quasi-periodic warm and cool patterns. The relative warm (cool) equatorial temperatures are mostly anti-correlated with cool (warm) temperatures at $\pm 12°$. The high variances of the data (f) at the equator and $\pm 12°$ shows that the QQO is most prominent at these latitudes. The brightness temperature as a function of time for the equatorial latitudes between $\pm 1°$ is shown in (g). The error bars shown in (g) represent the standard deviation of the average at each latitude of the zonal-mean brightness temperatures corresponding to observations taken on the same date. In the cases where a single image is available on a single observing night, we represent the errors as the root square of the estimated average absolute calibration uncertainty and the zonal variability (see Methods). Dashed white lines in (a-d) indicate $\pm 12°$ latitude.

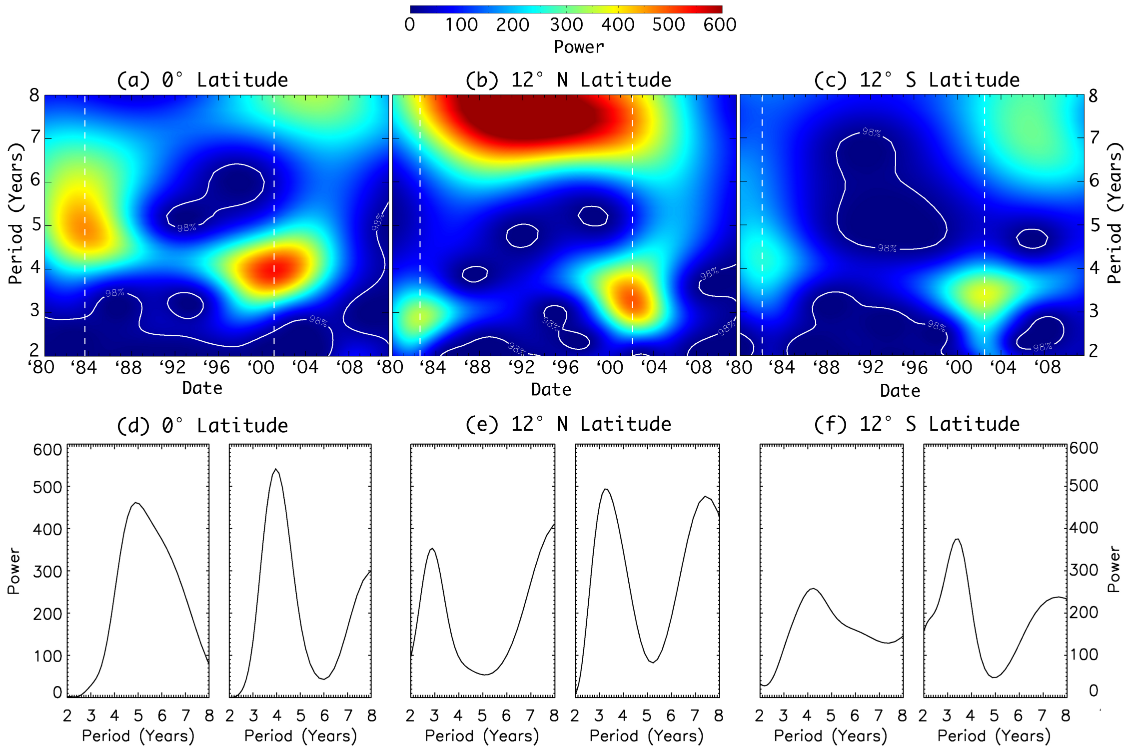

Figure 2: wavelet-transform periodogram of the ~ 7.9 μm brightness temperature between 1980 and 2012 (a-c) for the equatorial latitudes between $\pm 1°$ (a), and off-equatorial latitudes between 11-13° N (b) and 10-12° S (c), showing the period of the QQO as a function of time. Panels (d-f) represent the period of the QQO as a function of the power spectrum for the dates indicated by vertical white dashed lines in (a-c). The white contour lines in (a-c) indicate the 98% significance of the power spectrum.

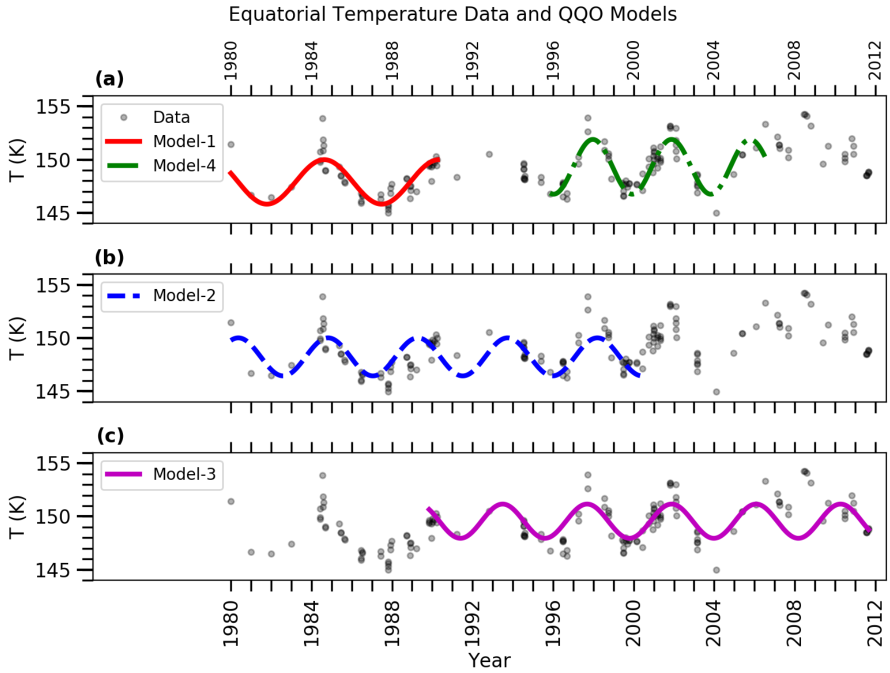

Figure 3: Models 1 (τ=5.7 yrs) and 4 (τ=3.9 yrs) fit their respective data very well with different QQO periods over the selected time spans (panel a). Models 2 (τ=4.5 yrs) and 3 (τ=4.2 yrs) have similar periods and while they fit the data well over certain dates, they fail to capture the dynamic QQO period over the entire data set. This is especially evident near 1988 with Model 2 and in 2008 for Model 3.

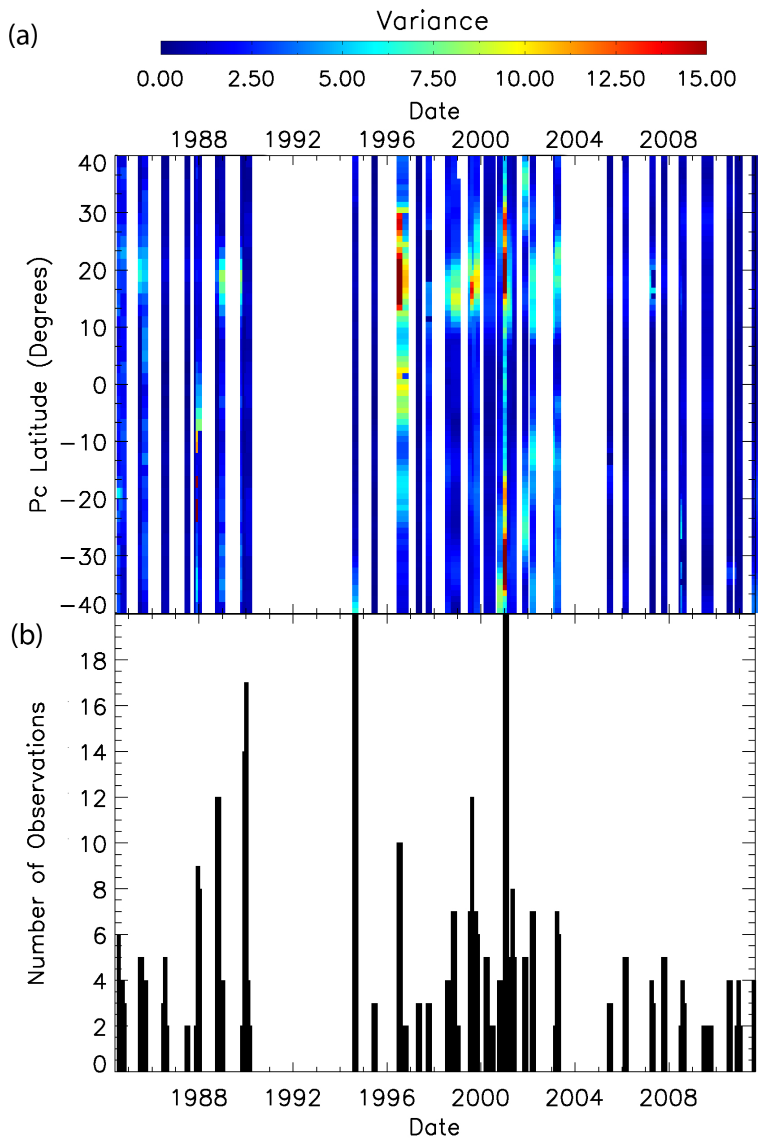

Figure 4: Longitudinal variance of the stratospheric brightness temperatures as a function of latitude and date (a), showing the presence of wave or vortex activity (high variance) mainly at $\sim 20°$ N. The variances shown here represent the maximum longitudinal variance found in 60-day intervals. The number of available images over the 60-day windows for each latitude are shown in (b). Note that small longitudinal variance is observed near 1990-1992 and 2007, when the QQO disruptions were observed. See Methods section for a detailed description of the methodology. White regions correspond to epochs with fewer than two observations.

Wavelet-Transform Analysis Results

Time Years	Lat (deg)	Period (yrs)
	Eq.	$5.0^{+1.8}_{-1.0}$
'80-90	12°N	$2.9^{+0.6}_{-0.6}$
	12°S	$4.2^{+1.0}_{-1.3}$
	Eq.	$3.9^{+0.7}_{-0.7}$
'96-06	12°N	$3.3^{+0.9}_{-0.6}$
	12°S	$3.3^{+0.6}_{-0.8}$

Modelling results

Time Years (Model No.)	Lat (deg)	Period (yrs)
	Eq.	$5.7^{+1.1}_{-0.8}$
'80-90 (1)	12°N	$7.3^{+3.7}_{-2.1}$
	12°S	$4.1^{+2.1}_{-1.0}$
	Eq.	$4.5^{+0.2}_{-0.2}$
'80-00 (2)	12°N	$4.4^{+0.3}_{-0.3}$
	12°S	$4.2^{+0.2}_{-0.2}$
	Eq.	$3.9^{+0.2}_{-0.2}$
'96-06 (4)	12°N	$3.7^{+0.6}_{-0.6}$
	12°S	$3.8^{+0.4}_{-0.4}$

Table 1: Periods of the equatorial and off-equatorial latitudes found for the 7.9-μm brightness temperatures by the wavelet-transform analysis (top) and by the non-linear Levenberg-Marquardt method (bottom). Both analyses return very similar results. The equatorial periods of the QQO found here are statistically unique.

Methods

Ground-Based Observations and Data Reduction

This study uses 7.6-7.9 μm images of Jupiter captured between 1980 and 2011 by five different instruments mounted at NASA's 3-m Infrared Telescope Facility (IRTF) on Maunakea, Hawai'i. The 7.6-7.9 μm radiance, originating from a pressure region spanning approximately 10-20 mbar in Jupiter's stratosphere (14), reveals the CH_4 emission and allows estimates of stratospheric temperatures. The ground-based observations used in this study include 1980-2000 data used in (14; 15; 16) and (17) as well as additional observations never published before. A summary of the dates and instruments are shown in Table A.1. A description of the different instruments is found in the previously mentioned references and references therein.

Raw MIRLIN, MIRAC and MIRSI data (1994-2011) are reduced using the Data Reduction Manager (DRM) software (see 42) written in the Interactive Data Language (IDL). The reduction technique includes the following steps: (i) subtraction of the sky emission using chop-nodded images; (ii) correction of the spurious pixels and non-uniformities in the detector by flat fielding; (iii) coadding multiple corrected images separated by less than an hour to increase the signal-to-noise ratio; (iv) geometric calibration of the images by limb-fitting; and (v) projection of the images as cylindrical maps of 0.5° x 0.5° (longitude-latitude) or 1° x 1° spatial resolution, depending on the quality of the image, to assign longitudes, latitudes and emission angles to each pixel. The BOLO-1 and AT1 data used in this study (captured between 1980-1981 and 1982-1992, respectively) were previously reduced and projected into 1° x 2° (longitude-latitude) cylindrical maps by (15). Information for these observations and reduction techniques are described in that paper.

To avoid radiometric calibration differences between the previously reduced and published data and the new data reduced in this study, we re-calibrated all the data in a systematic way. Each cylindrical map is radiometrically calibrated by scaling the radiance to match the Voyager IRIS and Cassini CIRS observations from 1979 and 2000, respectively, at mid-latitudes. To do so, we compute the zonal average of the radiance within 20° longitude around the central meridian for each latitude, creating a latitude-radiance profile for each cylindrical map. These profiles are then compared one by one to the zonally-averaged radiance of the IRIS and CIRS observations to obtain a scaling factor for each cylindrical map. This calibration technique has been widely used in previous studies and assumes that Jupiter's zonal average brightness at mid-latitudes remains mostly invariant with time (e.g. 42).

The reduced and calibrated data are then used to compute the 7.9-μm zonally-averaged brightness temperatures for each observing date. This is computed by binning the radiance corresponding to emission angles smaller than 75° of all images captured in a single observation night, in latitudinal bins of 1° and converting them to brightness temperatures. Radiances corresponding to emission angles greater than 75° are ignored from the average in order to avoid strong limb brightening and convolution of the edge of the planet's disc with deep space. Zonally-averaged brightness temperatures shown in this study might differ from those shown in (14; 17) as these previous studies used yearly brightness temperatures corresponding to annual-averages of the stratospheric zonal-mean temperatures.

The data reduction process introduces diverse systematic errors to the final radiance (brightness temperatures) from various sources. The largest uncertainties are introduced during the absolute radiometric calibration process due to (i) differences in the radiance between Voyager IRIS and Cassini CIRS that would lead to an overall 0.4 K difference in the temperatures between the older (1980s) and newer (1990s and 2000s) observations, and (ii) radiometric scaling error, which we estimate to be 0.95 K in the worst cases, less than 0.05 K in the best cases and 0.30 K in average. We estimate these uncertainties by looking for the scaling factor required to minimize differences in (i) the Voyager IRIS and Cassini CIRS final radiances, and (ii) the zonal mean brightnesses of different observations captured during a single night (and repeat this for all the available observing dates). Error bars shown in Figure 1 represent the standard deviation of the average at each latitude of the zonal-mean brightness temperatures corresponding to observations taken on the same date. This standard deviation includes not only the contribution from the longitudinal variability, but also accounts for the calibration uncertainty. In the cases where a single image is available on a single observing night we represent the errors as the root square of the estimated average radiometric scaling uncertainty and the zonal variability.

Date	**Instrument**	**Configuration**	**References**
1980 - 1981	BOLO-1	Raster-scanned	(14; 15; 16)
1982 - 1992	AT1	Raster-scanned	(14; 15; 16)
1994 - 1999	MIRAC	Full-frame	(17)
1996 - 2003	MIRLIN	Full-frame	Part in (17)
2003 - 2011	MIRSI	Full-frame	–

Table A.1: Summary of the dates, instruments and observation configurations of the data set used in this study.

Wavelet-Transform Analysis

In order to study the long-term periodicity of the Jovian Quasi-Quadrennial Oscillation we perform a wavelet-transform analysis. This is a powerful tool used to analyze potential changes within a time series (43). Unlike the Fourier transform or the Lomb-Scargle method (44), the wavelet-transform analysis provides accurate time-frequency analysis for signals where sinusoidal functions with a single frequency cannot reproduce the observations, by expanding a set of functions, called wavelets, given by the user. This technique is widely used in geophysics and has been previously used to analyzed the long-term variability of Jupiter's 1-4 bar level atmosphere (33). Here we follow (33) and use the most commonly used wavelet function, i.e. the Morlet wavelet, which consists of a plane wave modulated by a Gaussian (45; 46). This wavelet is defined as:

$$\phi\left(t\right) = \pi^{-1/4}\, e^{i\omega_0 t}\, e^{-t^2/2} \tag{A.1}$$

where ω_0 is a wavenumber and t is time.

In this study, we use in particular the 'wavelet.pro' code written in IDL (43). This function computes the 1D wavelet transform by translating and changing the wavenumber of the function given in equation 1 and allows the user to set a significance level to use. Here we set a significance level of 0.98. We also set the PAD keyword, which minimizes the errors introduced by the temporal boundaries of our data set. The time series analyzed by the wavelet-transform analysis must be evenly spaced in time. As our observations are not obtained on a regular basis, we interpolate the 7.9-μm radiance onto a regular grid of 2 days using a basic linear interpolation and then smooth the interpolated radiance with a boxcar average of 10 days. This grid provides the best representation of our data.

Non-linear Levenberg-Marquardt Analysis

We used a Non-Linear Least-Square Minimization and Curve-Fitting Python package `(DOI: 10.5281/zenodo.11813)` utilizing the Levenberg - Marquardt method to find the best sinusoidal modeled amplitude, period, phase, and offset constant given by,

$$\text{Model} = A\, \sin\left(2\pi\frac{t}{\tau} + \phi\right) + C \tag{A.2}$$

where A is the amplitude, t is time, τ is the QQO period, ϕ is the phase, and C is a constant or the approximate mean temperature of observational data spanned by the model for a specific latitude. Four time intervals were chosen to model the equatorial and $\pm 13^\circ$ latitude regions, allowing us to compare the derived QQO periods to previous research and to each other to investigate the temporal evolution of the QQO: (i) Model 1 fit data between 1980 and 1990; (ii) Model 2 fit data between 1980 and the Cassini mission Jupiter flyby in late 2000; (iii) Model 3 reproduced data between 1990 and 2011; and (iv) Model 4 examined data between 1996 and 2006.

In order to establish the significance in the results of our fitted models to the data, we varied the range of data included in both Models 1 and 4. The indices of the equatorial data for Models 1 and 4 presented throughout this paper are 0-49 and 63-130, respectively. We rooted the beginning of the observations because of how sparse the data is around 1980-1983, so the 0 index position was held constant. In order to be systematic in this analysis, the same initial conditions for Model 1 and Model 4 were used while the indices were altered from the base values presented earlier. The internal Levenberg - Marquardt method parameters such as tolerance, iteration limits, and the "throttle" lambda variable were also held constant in this exploration.

The indices for Model 1 were varied by ± 1 which produced an increase in the period uncertainty by 20% while the period itself did not change. Extending Model 1 to include points later in time did not find converged solutions, most likely caused by the spacing of data points between 1991-1994. The indices for Model 4 were varied by ± 10 and over this range, the QQO model period varied within the range of 3.84-4.22 years with an uncertainty range of 0.1-0.56 years. When leaving Model 1 constant, these variations in Model 4 data produced p-test probabilities that varied in the range of 1.11-3.77%.

Longitudinal Variance Analysis

To investigate potential sources responsible for the observed QQO disruptions around 1992 and late 2007, we searched for hot stratospheric vortices and strong stratospheric wave activity that, like on Saturn, could have disrupted the stratospheric temperature oscillations. One way to do this is by analyzing how the 7.9-μm brightness temperatures vary with longitude and date, as localized stratospheric vortices and wave activity would result in large longitudinal variability of the brightness temperature.

In this study, we first compute the variance at longitudes within $\pm 40°$ of the central meridian for each latitude and date. However, due to the different observing settings used and the very different weather conditions during each of the observing runs, global maps of Jupiter were not always acquired, resulting in cases where the presence of vortices or wave activity could have been missed because we were viewing a 'quiet' side of Jupiter. To try to solve this problem, we search for the largest variance at each latitude using a 60-day temporal resolution boxcar. In most cases, this temporal resolution is long enough to have at least two images available. Epochs where only one image is available in a 60-day window are not taken into account. This solution only partially addresses the problem as there is always a small chance that the available images in a 60-day window span similar longitudes, but is the best that can be done with this limited dataset. To analyze the robustness of the obtained results we show the number of images available at each latitude over the 60-day windows in Figure 4.